ARTICLES
https://doi.org/10.1038/s41929-022-00798-z

nature catalysis

OPEN

Deep learning-based k_{cat} prediction enables improved enzyme-constrained model reconstruction

Feiran Li[1,4], Le Yuan[1,2,4], Hongzhong Lu[1], Gang Li[1], Yu Chen[1], Martin K. M. Engqvist[1], Eduard J. Kerkhoven[1,2] ✉ and Jens Nielsen[1,3]

Enzyme turnover numbers (k_{cat}) are key to understanding cellular metabolism, proteome allocation and physiological diversity, but experimentally measured k_{cat} data are sparse and noisy. Here we provide a deep learning approach (DLKcat) for high-throughput k_{cat} prediction for metabolic enzymes from any organism merely from substrate structures and protein sequences. DLKcat can capture k_{cat} changes for mutated enzymes and identify amino acid residues with a strong impact on k_{cat} values. We applied this approach to predict genome-scale k_{cat} values for more than 300 yeast species. Additionally, we designed a Bayesian pipeline to parameterize enzyme-constrained genome-scale metabolic models from predicted k_{cat} values. The resulting models outperformed the corresponding original enzyme-constrained genome-scale metabolic models from previous pipelines in predicting phenotypes and proteomes, and enabled us to explain phenotypic differences. DLKcat and the enzyme-constrained genome-scale metabolic model construction pipeline are valuable tools to uncover global trends of enzyme kinetics and physiological diversity, and to further elucidate cellular metabolism on a large scale.

The enzyme turnover number (k_{cat}), which defines the maximum chemical conversion rate of a reaction, is a critical parameter for understanding the metabolism, proteome allocation, growth and physiology of a certain organism[1–3]. There are large collections of k_{cat} values available in the enzyme databases BRENDA[4] and SABIO-RK[5], which are, however, still sparse compared to the variety of existing organisms and metabolic enzymes, largely due to the lack of high-throughput methods for k_{cat} measurement. Additionally, experimentally measured k_{cat} values have considerable variability due to varying assay conditions such as pH, cofactor availability and experimental methods[6]. Altogether, the sparse collection and considerable noise limit the use of k_{cat} data for global analysis and may mask enzyme evolution trends.

In particular, enzyme-constrained genome-scale metabolic models (ecGEMs), where the whole-cell metabolic network is constrained by enzyme catalytic capacities and thereby able to accurately simulate the maximum growth abilities, metabolic shifts and proteome allocations, rely heavily on genome-scale k_{cat} values[2,7]. Over the past decade, ecGEMs (or models following the concept of enzyme constraints) have been separately developed for several well-studied organisms[7] including *Escherichia coli*[8,9], *Saccharomyces cerevisiae*[2,10], Chinese hamster ovary cells[11] and *Homo sapiens*[12]. Due to the limitations of k_{cat} measurements[13] and the reliance on enzyme commission (EC) number annotations to search for k_{cat} values in those developed pipelines[2,8,10], the reconstruction of ecGEMs for lesser-studied organisms or large-scale reconstruction for multiple organisms has remained a challenge[7,14]. Moreover, even for those well-studied organisms, the k_{cat} coverage is far from complete[13,15,16]. In a *S. cerevisiae* ecGEM, only 5% of all enzymatic reactions have fully matched k_{cat} values in BRENDA[2]. When data are missing, previous ecGEM reconstruction pipelines typically assume k_{cat} values from similar substrates, reactions or other organisms, which can result in model predictions deviating from experimental observations[7]. There is a clear requirement for obtaining large-scale k_{cat} values to improve model accuracy and yield more reliable phenotype simulations[17].

Deep learning has been applied and shown great performance in modelling chemical spaces[18], gene expression[19], enzyme-related parameters such as enzyme affinity[20] and EC numbers[21]. Previously, Heckmann and colleagues employed machine learning approaches to predict *E. coli* k_{cat} values based on features such as average metabolic fluxes and catalytic sites obtained from protein structures[16]. However, such features are typically hard to obtain, which allows the application of this approach only to the most well-studied organisms such as *E. coli*.

To this end, we developed a deep learning approach (DLKcat) that uses substrate structures and protein sequences as inputs, and demonstrated its capability for the large-scale prediction of k_{cat} values for various organisms, as well as for identifying key amino acid residues that affect these predictions. We showcased the predictive power of the deep learning model by predicting genome-scale k_{cat} profiles for 343 yeast/fungi species, accounting for more than 300,000 enzymes and 3,000 substrates. The predicted k_{cat} profiles enabled reconstruction of 343 ecGEMs for the yeast/fungi species through an automatic Bayesian-based pipeline, which can accurately simulate growth phenotypes among yeast species and identify the phenotype-related key enzymes.

Results

Construction of a deep learning approach for k_{cat} prediction. The deep learning approach DLKcat was developed by combining a graph neural network (GNN) for substrates and a convolutional neural network (CNN) for proteins (Fig. 1). Substrates were represented as molecular graphs converted from the simplified

[1]Department of Biology and Biological Engineering, Chalmers University of Technology, Gothenburg, Sweden. [2]Novo Nordisk Foundation Center for Biosustainability, Chalmers University of Technology, Gothenburg, Sweden. [3]BioInnovation Institute, Copenhagen, Denmark. [4]These authors contributed equally: Feiran Li, Le Yuan. ✉e-mail: eduardk@chalmers.se

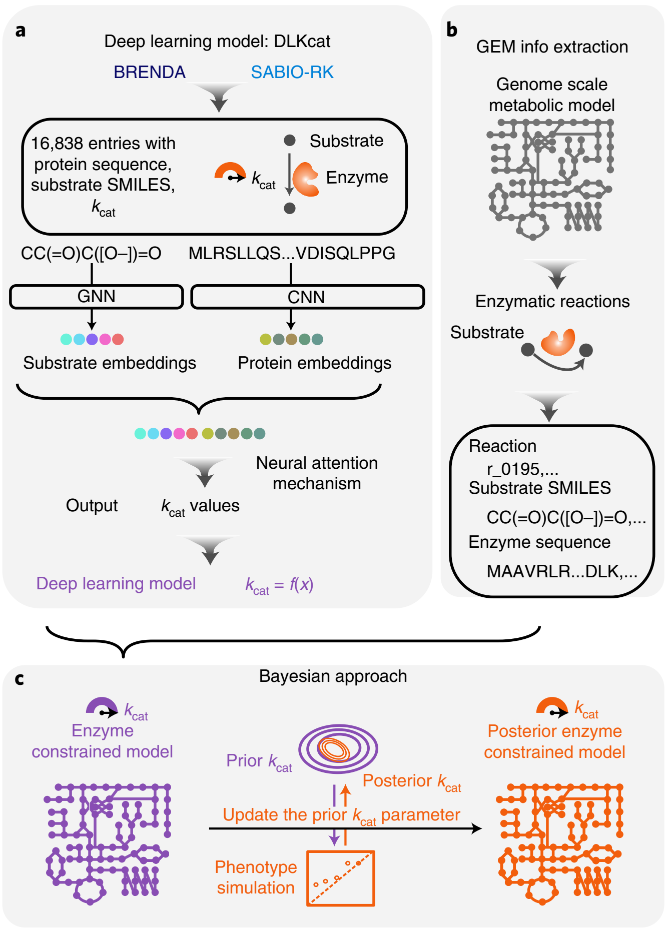

Fig. 1 | Deep learning of k_{cat} for ecGEM parameterization. a, DLKcat, the approach developed for k_{cat} prediction by combining a GNN for substrates and a CNN for proteins. **b**, Information extraction from GEMs as the input for the deep learning model to predict k_{cat} values. **c**, The developed Bayesian facilitated pipeline to reconstruct ecGEMs using the predicted k_{cat} profiles from the deep learning model.

molecular-input line-entry system (SMILES), and protein sequences were split into overlapping *n*-gram amino acids (the string of contiguous sequences consisting of *n* items). We generated a comprehensive dataset from the BRENDA[4] and SABIO-RK[5] databases to train the neural network. Incomplete database entries with missing information and redundant entries were filtered out to ensure a dataset of unique entries with substrate name, substrate SMILES information, EC number, protein sequence, organism name and k_{cat} value. The final dataset contained 16,838 unique entries catalysed by 7,822 unique protein sequences from 851 organisms and converting 2,672 unique substrates (Supplementary Figs. 1 and 2). This dataset was randomly split into training, validation and test datasets by 80%, 10% and 10%, respectively, while five times of random splitting indicated the robustness of the deep learning model (Supplementary Fig. 3).

Deep learning model performance for k_{cat} prediction. The effects of hyperparameters on deep learning performance were evaluated by learning curves (Supplementary Fig. 4). With the selected optimal parameters (*r*-radius substrate subgraphs, in which *r* is the number of hops from a vertex of substrate structure, 2; *n*-gram amino acids, 3; vector dimensionality, 20; time steps in GNN, 3; number of layers in CNN, 3), the deep learning model was trained. The root mean square error (r.m.s.e.) of k_{cat} predictions gradually decreased with increasing epoch (Fig. 2a), where one epoch is one iteration of the dataset passing through the neural network. A final deep learning model trained and stored for further use had a r.m.s.e. of 1.06 for the test dataset, signifying that predicted and measured k_{cat} values were overall within one order of magnitude (Fig. 2a). A high predictive accuracy could be observed on both the whole dataset (training, validation and test datasets) (Fig. 2b; Pearson's $r = 0.88$) and the test dataset (Supplementary Fig. 5a; Pearson's $r = 0.71$; Supplementary Fig. 5b for test dataset where at least either the substrate or enzyme was not present in the training dataset; Pearson's $r = 0.70$). The predicted k_{cat} values were categorized according to the metabolic context of the enzymes (Supplementary Table 1), and enzymes involved in primary central and energy metabolism yielded significantly higher k_{cat} values than enzymes involved in intermediary and secondary metabolism (Supplementary Fig. 5c), in agreement with previous observations[6].

The deep learning model was able to show enzyme promiscuity. Understanding enzyme promiscuity and the related underground metabolism is a key topic in evolutionary biology[22,23]. DLKcat-predicted k_{cat} values (Fig. 2c) were higher for preferred substrates (median $k_{cat} = 11.07\,s^{-1}$) compared to alternative substrates (median $k_{cat} = 6.01\,s^{-1}$; $P = 1.3 \times 10^{-12}$) and random substrates (median $k_{cat} = 3.51\,s^{-1}$; $P = 9.3 \times 10^{-6}$) for promiscuous enzymes in the whole dataset, while the same trend was identified in the test dataset (Supplementary Fig. 5d; $P < 0.05$). The concept of native and underground metabolism[24] could be exemplified with the rich experimental k_{cat} data that are available for human aldo–keto reductase and 61 substrates, where DLKcat could differentiate (Fig. 2d; $P = 0.0039$) between native (top 10% experimental k_{cat} values, median $= 2.22\,s^{-1}$) and underground (last 10%, median $= 0.04\,s^{-1}$) substrates.

Prediction and interpretation of k_{cat} of mutated enzymes. Beyond good overall performance (Fig. 2b), DLKcat was able to capture the effects of amino acid substitutions on the k_{cat} values of individual enzymes. The annotated dataset was divided into wild-type enzymes and mutated enzymes with amino acid substitutions. As the median k_{cat} of mutant enzymes was lower than that of wild-type enzymes (Supplementary Fig. 6a), the deep learning model was a good k_{cat} predictor for both wild-type enzymes (Fig. 3a for the whole dataset; Pearson's $r = 0.87$; Supplementary Fig. 6b for the test dataset; Pearson's $r = 0.65$) and mutated enzymes (Fig. 3b for the whole dataset; Pearson's $r = 0.90$; Supplementary Fig. 6c for the test dataset; Pearson's $r = 0.78$). Several well-studied enzyme–substrate pairs were collected from the literature, where each pair had k_{cat} values reported for at least 25 unique single or multiple amino acid substitutions (Supplementary Table 2). The predicted and experimentally measured k_{cat} values correlated very well (Pearson's $r = 0.94$; Fig. 3c). The experimentally measured k_{cat} values were further grouped as within a 0.5-fold to 2.0-fold change of wild-type k_{cat} ('wild-type-like k_{cat}') or less than a 0.5-fold change of wild-type k_{cat} ('decreased k_{cat}'). The scarcity of mutated enzymes with k_{cat} values over twofold of the wild-type k_{cat} values precluded defining the 'increased k_{cat}' group[25,26]. DLKcat was able to capture the effects of small changes in protein sequences on the activities of individual enzymes, as the decreased k_{cat} group contained significantly lower predicted k_{cat} values compared to the wild-type-like k_{cat} group, for all enzyme–substrate pairs (Fig. 3d).

To investigate which amino acid residues dominate enzyme activity, we applied a neural attention mechanism to back-trace important signals from the neural network output towards its input[27]. This approach assigns attention weights to each amino acid residue, quantitatively describing its importance for the predicted enzyme activity. Attention weights were calculated for the wild-type *H. sapiens* purine nucleoside phosphorylase (PNP) with inosine as substrate, as rich mutation data are available for this enzyme–substrate

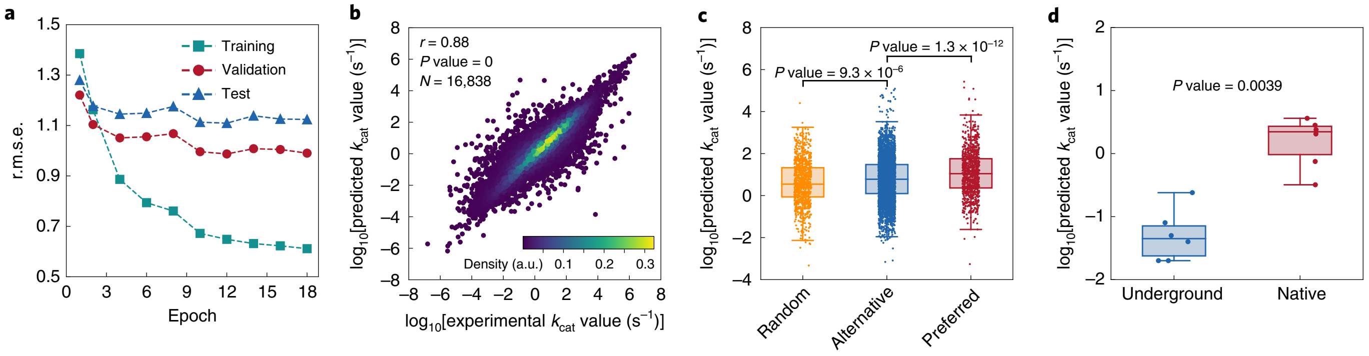

Fig. 2 | Deep learning model performance for k_{cat} prediction. **a**, The r.m.s.e. of k_{cat} prediction during the training process. **b**, Performance of the final deep learning model. The correlation between predicted k_{cat} values and those present in the whole dataset (training, validation and test datasets) was evaluated. The brightness of colour represents the density of data points. Student's *t*-test was used to calculate the *P* value for Pearson's correlation. **c**, Enzyme promiscuity analysis on the whole dataset. For enzymes with multiple substrates, we divided the substrates into preferred and alternative by their experimentally measured k_{cat} value, and then used the predicted k_{cat} values for this box plot. Random substrates were randomly chosen from the compound dataset in our training data, except for the documented substrates and products for the tested enzyme. We evaluated 945 promiscuous enzymes in the whole dataset ($n=945$ for preferred substrates, $n=4,238$ for alternative substrates, $n=945$ for random substrates). **d**, Comparison of the predicted k_{cat} values for the native substrates and the underground substrates with the human aldo–keto reductase enzyme as a case study. Here, we defined those substrates with the top 10% catalytic ability (experimental k_{cat} value) as the native substrates ($n=6$), while those with the last 10% catalytic ability (experimental k_{cat} value) were considered as the underground substrates as defined in the reference ($n=6$)[24]. In each box plot (**c** and **d**), the central band represents the median value, the box represents the upper and lower quartiles and the whiskers extend up to 1.5 times the interquartile range beyond the box range. A two-sided Wilcoxon rank sum test was used to calculate the *P* values in **c** and **d**.

pair[28] (Fig. 3e and Supplementary Table 3). Situating the mutations from the wild-type-like k_{cat} and decreased k_{cat} groups (Fig. 3e) to the wild-type PNP sequence exhibited that residues that were mutated in the decreased k_{cat} group had significantly higher attention weights (Fig. 3f; $P=0.0014$; Supplementary Table 4). The calculation of attention weights from the deep learning model can thereby identify amino acid residues whose mutation would likely have a more substantial effect on enzyme activity.

The k_{cat} prediction for 343 yeast/fungi species. We previously reconstructed GEMs for 332 yeast species plus 11 out-group fungi, but only expanded 14 of them to ecGEMs using the original pipeline[10] due to the limited available k_{cat} data[14]. As DLKcat allows prediction of almost all k_{cat} values for metabolic enzymes against any substrates for any species, this enabled the generation of ecGEMs for all 343 yeast/fungi species, predicting k_{cat} values for around three million enzyme–substrate pairs (Supplementary Fig. 7). Yeast and fungal specialist enzymes (with narrow substrate specificity) had higher k_{cat} values compared with generalist (that is, promiscuous) enzymes that catalyse more than one reaction in the model (Supplementary Fig. 8a). This is aligned with the hypothesis that ancestral enzymes with broad substrate specificity and low catalytic efficiency improve their k_{cat} value when they evolve into specialists through mutation, gene duplication or horizontal gene transfer[29]. Sequence conservation also trended with predicted k_{cat} values, where the ratio of non-synonymous over synonymous substitutions (d*N*/d*S*) is commonly used to detect proteins undergoing adaptation[30]. Conserved enzymes with lower d*N*/d*S* have significantly higher k_{cat} values compared with relatively lesser conserved enzymes (with high d*N*/d*S*), implying that conserved yeast/fungi enzymes under evolutionary pressure are adapted to have higher k_{cat} values (Supplementary Fig. 8b).

Bayesian approach for 343 ecGEM reconstructions. Using the predicted k_{cat} values for 343 yeast/fungi species, we generated 343 'DL-ecGEMs' (ecGEMs parameterized with k_{cat} values from DLKcat). The training data for the deep learning model were primarily measured in vitro, which implies that DLKcat also predicts in vitro k_{cat} values, which is undesired as in vitro k_{cat} values can be considerably different from in vivo[31]. To resolve these uncertainties, we adopted a Bayesian genome-scale modelling approach[32]. Here, we used predicted k_{cat} values as mean values for prior distributions and experimentally measured phenotypes to update these to obtain posterior k_{cat} distributions. For this, experimental growth data on yeast/fungi species were collected, collating 371 entries for 53 species with 16 carbon sources (Supplementary Table 5 and Supplementary Fig. 9). A sequential Monte-Carlo-based approximate Bayesian computation (SMC-ABC) approach[32] was implemented to sample the k_{cat} values, after validating its generality with the ecGEM of *S. cerevisiae*, which had the most abundant experimental data (Supplementary Fig. 10). The ecGEMs parameterized with the mean values of sampled posterior k_{cat} values are hereafter represented as posterior-mean-DL-ecGEMs.

The Bayesian learning processes for *S. cerevisiae* and nonconventional yeast *Yarrowia lipolytica* are shown as examples (Fig. 4 and Supplementary Fig. 11). We calculated r.m.s.e. values between measurements and predictions for batch and chemostat growth of *S. cerevisiae* and *Y. lipolytica* under different carbon sources. After several generations, the ecGEMs parameterized with sampled posterior k_{cat} values achieved a r.m.s.e. lower than one (Fig. 4a and Supplementary Fig. 11a), which showed they could accurately describe the experimental observations. For instance, the *S. cerevisiae* ecGEM captured the metabolic shift at increasing growth rate (Fig. 4b)—known as the Crabtree effect[33]—while *Y. lipolytica* respired at its maximum growth rate (Supplementary Fig. 11b). Principal component analysis for all generated k_{cat} sets (9,800 sets for *S. cerevisiae* and 4,900 sets for *Y. lipolytica*) showed a gradual move from the prior distribution to the distinct posterior distribution (Fig. 4c and Supplementary Fig. 11c). The Bayesian learning process affected more variance than mean predicted k_{cat} values (Fig. 4d,e). For *S. cerevisiae*, 1,057 enzyme–substrate pairs reduced their k_{cat} variance (Šidák-adjusted one-tailed *F*-test, $P<0.01$), while only 532 pairs changed their mean predicted k_{cat} (Šidák-adjusted Welch's *t*-test, $P<0.01$), which were randomly distributed across metabolic subsystems (Supplementary Table 6; two-sided Fisher's exact test, $P>0.25$). For *Y. lipolytica*, the values were 1,224 and 646

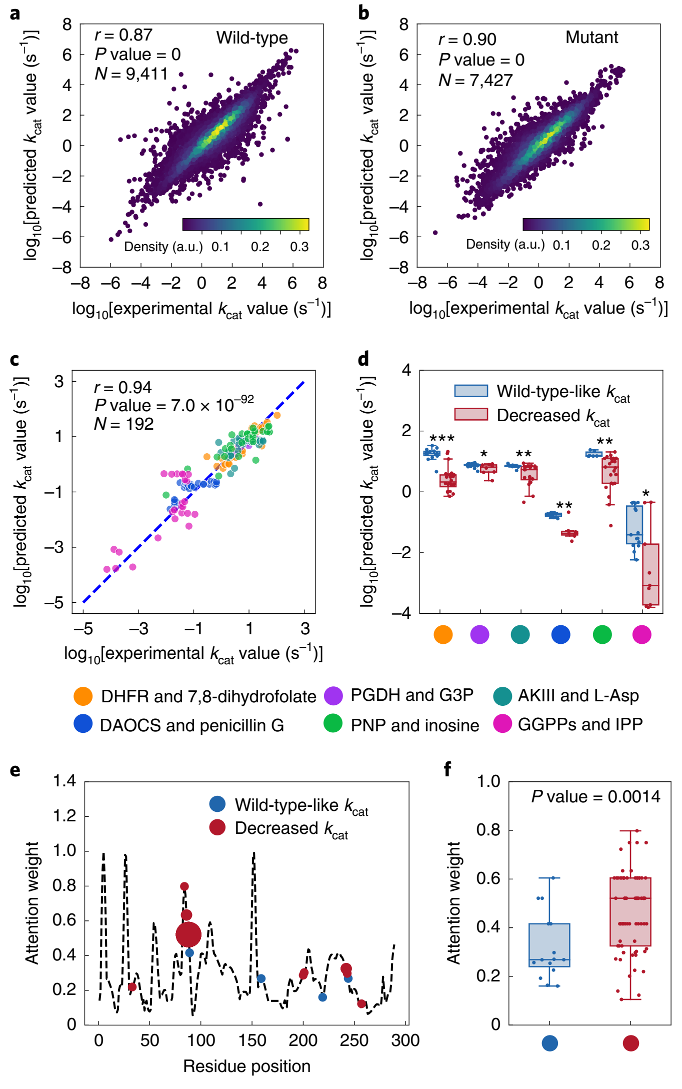

Fig. 3 | Deep learning model for the prediction and interpretation of k_{cat} of mutated enzymes. a,b, Prediction performance of k_{cat} values for all wild-type (**a**) and mutated (**b**) enzymes. Colour brightness represents data density. **c**, Comparison between predicted and measured k_{cat} values for several well-studied enzyme–substrate pairs with rich experimental mutagenesis data. Enzyme abbreviations: DHFR, dihydrofolate reductase; PGDH, D-3-phosphoglycerate dehydrogenase; AKIII, aspartokinase III; DAOCS, deacetoxycephalosporin C synthase; PNP, purine nucleoside phosphorylase; GGPPs, geranylgeranyl pyrophosphate synthase. Substrate abbreviations: G3P, glycerate 3-phosphate; L-Asp, L-aspartate; IPP, isopentenyl diphosphate. In **a**–**c**, the student's *t*-test was used to calculate the *P* value for the Pearson's correlation. **d**, Comparison of predicted k_{cat} values on several mutated enzyme–substrate pairs between enzymes with wild-type-like k_{cat} and decreased k_{cat}. $P < 0.05$ (*), $P < 0.01$ (**) and $P < 0.001$ (***), two-sided Wilcoxon rank sum test. Detailed information and sample numbers can be found in Supplementary Table 2. **e**, Attention weight of residue position in the wild-type PNP enzyme, using inosine as substrate. The mutated residues in each of the mutated enzymes (with both wild-type-like k_{cat} and decreased k_{cat}) were marked on the curve according to their mutated residue. Dot size indicates the number of mutated enzymes with mutations of that residue. **f**, Overall attention weights for the PNP–inosine pair, comparing enzymes with wild-type-like k_{cat} and decreased k_{cat} by two-sided Wilcoxon rank sum test. $n = 15$ for wild-type-like k_{cat}; $n = 72$ for decreased k_{cat}. In each box plot (**d** and **f**), the central band represents the median value, the box represents the upper and lower quartiles and the whiskers extend up to 1.5 times the interquartile range beyond the box range.

(Supplementary Fig. 11d,e). Consequentially, the sampled posterior k_{cat} values had a strong correlation with the deep learning-predicted k_{cat} values (Pearson's $r = 0.86$ for *S. cerevisiae*; Fig. 4f; Pearson's $r = 0.83$ for *Y. lipolytica*; Supplementary Fig. 11f).

Deep learning and Bayesian approaches improve ecGEM quality. We subsequently generated posterior-mean-ecGEMs from corresponding DL-ecGEMs for all the 343 yeast/fungi species. For comparison, we also built 'original-ecGEMs' for the same species with a k_{cat} parameterization strategy that assigns measured k_{cat} values from BRENDA[4] and SABIO-RK[5] to enzyme/reaction pairs as was done in previous pipelines[2,8]. We were able to reconstruct original-ecGEMs for all 343 yeast/fungi species only after assuming that orthologs across yeast species had the same EC number annotation as in *S. cerevisiae*. In case of missing data, certain flexibility was introduced by matching the k_{cat} value to other substrates or organisms, or even introducing wild cards in the EC number. The original-ecGEMs yielded k_{cat} values for ~40% of enzymes and generated enzymatic constraints for ~60% of enzyme-annotated reactions, while DL-ecGEMs and their derived posterior-mean-ecGEMs covered k_{cat} values for ~80% of enzymes and defined enzymatic constraints for ~90% of enzymatic reactions (Fig. 5a,b for 343 yeast/fungi species; Supplementary Fig. 12a,b for *S. cerevisiae*). While original-ecGEMs had fewer assigned k_{cat} values, their reconstruction pipeline also relied heavily on correct enzyme EC number annotations and available measured k_{cat} values in the databases, contrasting with the DL-ecGEM reconstruction, which relied only on protein sequences and substrate SMILES information while resulting in a higher coverage. In DL-ecGEMs and posterior-mean-ecGEMs the only missing k_{cat} values were for generic substrates without defined SMILES information (such as generic compounds phosphatidate and thioredoxin).

Besides the improved k_{cat} coverage, the posterior-mean-ecGEMs and DL-ecGEMs also outperformed original-ecGEMs in the prediction of exchange rates (Fig. 5c for 53 species with reported phenotype; Supplementary Fig. 12c for *S. cerevisiae*) and maximum growth rates under various carbon sources and oxygen availabilities (Fig. 5d and Supplementary Fig. 13 for 53 species with reported growth phenotype; Supplementary Fig. 12d for *S. cerevisiae*). Moreover, we used these three types of ecGEMs to predict required protein abundances and compared this with published quantitative proteomics data from four species with different carbon sources, culture modes and medium set-ups (Supplementary Table 7). Proteome predictions from DL-ecGEMs and posterior-mean-ecGEMs had the lowest r.m.s.e. values, while DL-ecGEMs had already reduced the r.m.s.e. by 30% when compared to original-ecGEMs (Fig. 5e for four species with absolute proteome data). Combined, the current pipeline not only increases k_{cat} coverage but also contributes to ecGEMs better representing the 343 fungi/yeast species.

The k_{cat} comparison identifies phenotype-related enzymes. The predicted k_{cat} values were furthermore able to distinguish between Crabtree positive and negative yeast species. There is much interest in understanding the presence of the Crabtree phenotype among yeast species[34,35], and a model of *S. cerevisiae* energy metabolism has previously been used to interpret this phenotype by comparing protein efficiency (that is, ATP produced per protein mass per time) in its two energy-producing pathways[1]. It was postulated that the Crabtree effect is related to the high-yield (HY) pathway (containing the Embden–Meyerhof–Parnas pathway, the tricarboxylic acid (TCA) cycle and the electron transport chain), having a lower protein efficiency than the low-yield (LY) pathway (containing Embden–Meyerhof–Parnas plus ethanol formation; Fig. 6a)[1]. We here used the posterior-mean-ecGEMs of 102 yeast species with experimental reported Crabtree phenotype (25 positive; 77 negative) to similarly calculate the protein efficiencies of the HY and LY

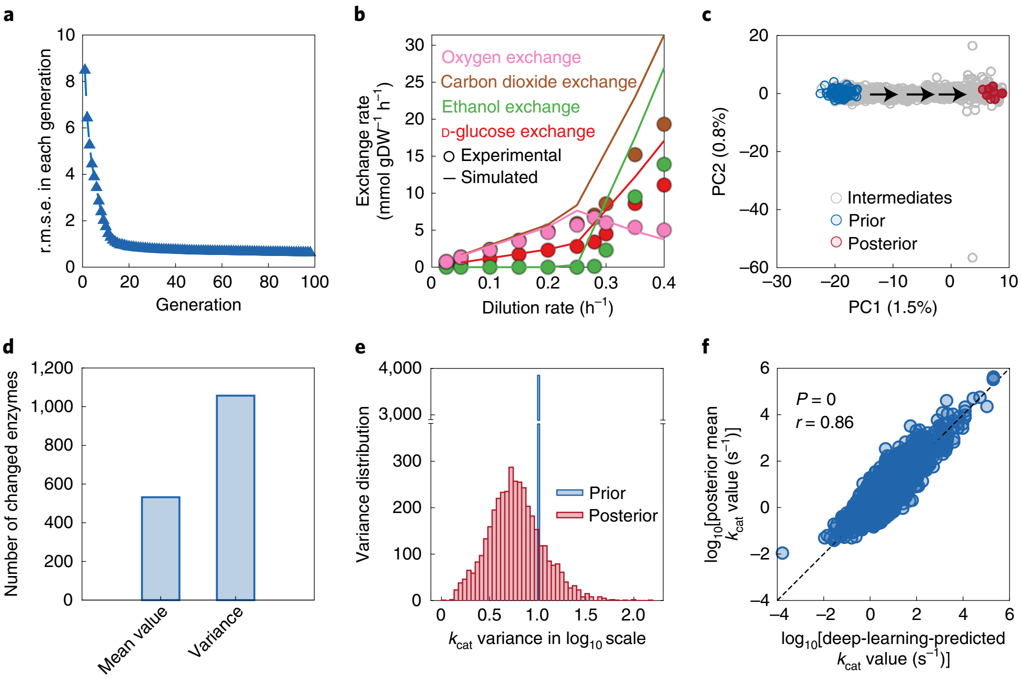

Fig. 4 | Bayesian modelling training performance for *S. cerevisiae* ecGEM. **a**, The r.m.s.e. for phenotype measurement and prediction during the Bayesian training process. **b**, Simulated exchange rates by posterior-mean-ecGEM (lines) compared with experimental data (dots). The k_{cat} values in the posterior-mean-ecGEMs are mean values from 100 sampled posterior datasets obtained from the Bayesian training process. **c**, Principal component analysis for k_{cat} datasets sampled during the Bayesian training approach, showing the progression from prior to posterior dataset. Each parameter in the set was standardized by subtracting the mean and then divided by the standard deviation before the principal component analysis. In blue are 100 sampled prior datasets; in red are 100 sampled posterior datasets; in grey are all other intermediate datasets. PC, principal component. **d**, The number of enzymes with a significantly changed mean value (Šidák-adjusted Welch's *t*-test, $P < 0.01$, two-sided) and variance (Šidák-adjusted one-tailed *F*-test, $P < 0.01$) between the sampled prior and posterior k_{cat} datasets. Parameters from 126 prior and 100 posterior ecGEMs were used for statistical tests. **e**, Variance distribution comparison for prior and posterior distribution. **f**, Correlation between deep learning-predicted k_{cat} and posterior mean k_{cat}. Student's *t*-test was used to calculate *P* value for Pearson's correlation.

pathways. Of the 102 species, 89% followed the trend that Crabtree positive species have a higher LY efficiency, suggesting that Crabtree positive yeasts' LY pathways are more protein efficient than their HY pathways for producing the same amount of ATP (Supplementary Table 8). For five commonly studied species, the results are shown in Fig. 6b, and even though ATP yields in their HY pathways may vary across species, primarily due to the presence of respiratory complex I, they still followed the same trend (Supplementary Table 8). Inconsistencies in strains where the HY/LY protein efficiency ratio did not trend with the Crabtree effect might be due to additional regulation not considered in ecGEMs[36].

With the predicted k_{cat} profiles for yeast species, we could investigate whether key enzymes show different k_{cat} values among 25 Crabtree positive and 77 negative species. Of the enzymes in the energy-producing pathways, only pyruvate kinase, citrate synthase, fumarase and phosphoglucose isomerase had significantly different k_{cat} values (Fig. 6c). Since fumarase and phosphoglucose isomerase can operate in reversible directions, it is unclear how the k_{cat} difference relates to the Crabtree effect. The k_{cat} values of pyruvate kinase were higher in Crabtree positive species ($P = 0.006$; Fig. 6c). This aligns with the fact that increasing pyruvate kinase activity in the Crabtree positive *Schizosaccharomyces pombe* increases its fermentation ratio, decreases the growth dependence on respiration and provides resistance to growth-inhibiting effects of antimycin A, which inhibits respiratory complex III (ref. [37]). Citrate synthase catalyses the first and rate-limiting step of the TCA cycle[38], condensing acetyl-coenzyme A and oxaloacetate to citrate. The k_{cat} values of citrate synthase of Crabtree negative species are higher ($P = 0.008$), which would benefit metabolic flux from entering the TCA cycle (Fig. 6a,c). This is consistent with ^{13}C-metabolic flux analysis that showed that Crabtree negative species have higher TCA flux[39,40].

Discussion

The diversity of biochemical reactions and organisms makes it difficult to generate genome-scale k_{cat} profiles. Here we presented the deep learning approach DLKcat to predict k_{cat} values of all metabolic enzymes against their substrates, requiring only the substrate SMILES information and protein sequences of the enzymes as input, yielding a versatile k_{cat} prediction tool for any species.

DLKcat can capture k_{cat} changes towards precise single amino acid substitutions, enabling attention weight calculations that identify the amino acid residues majorly impacting enzyme activity. Amino acid substitution is a powerful technique in the enzyme evolution field and routinely used to probe enzyme catalytic mechanisms[41,42]. Particularly, most substitution experiments perform mutagenesis in the substrate binding site region, since it is hypothesized that the binding region would have a high impact towards catalytic activity. However, it has been reported that remote regions can have a profound impact on catalytic activity[43,44]. Here, we identified not only high attention weights for amino acid residues in the inosine binding region of human PNP enzyme, but also various non-binding residue sites with high attention weights, suggesting that those residues may also majorly impact catalytic activity and deserve further validation. DLKcat can thereby serve as a valuable part of the protein engineering toolbox[45,46].

Predicted genome-scale k_{cat} profiles can facilitate the reconstruction of enzyme-constrained models of metabolism, from both curated and automatically generated basic (non-ec) GEMs. The

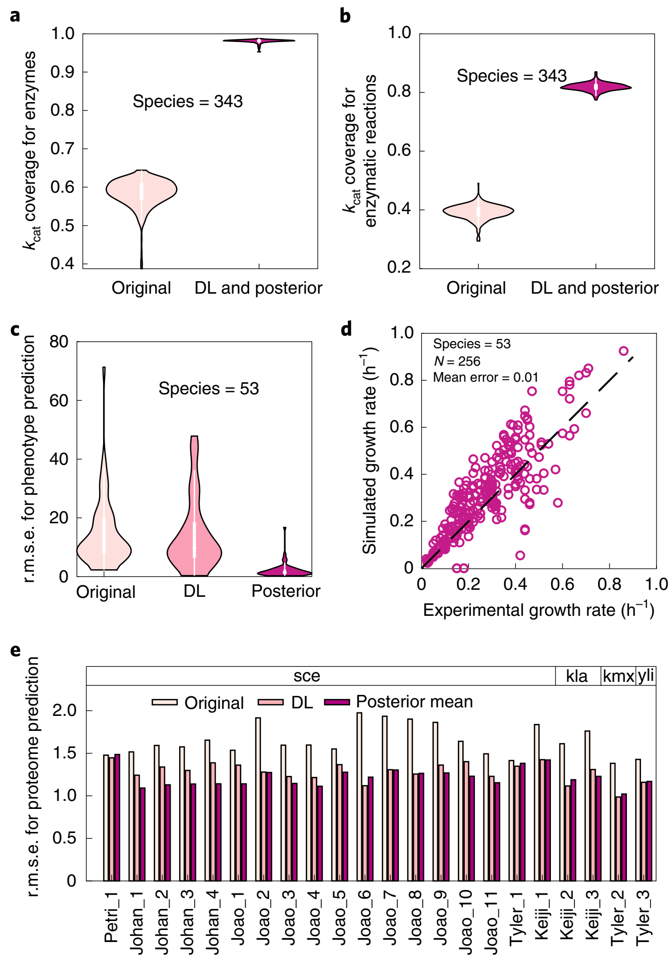

Fig. 5 | Evaluation of three ecGEM modelling pipelines including original-ecGEM, DL-ecGEM and posterior-mean-ecGEM reconstruction. **a**,**b**, Enzymatic constraint coverage comparison for enzymes (**a**) and enzymatic reactions (**b**) of 343 yeast/fungi species. **c**, The r.m.s.e. for the phenotype prediction for 53 species with phenotype data. **d**, Growth prediction of posterior-mean-ecGEMs for 53 species with phenotype data. **e**, Performance of three types of ecGEMs in predicting quantitative proteome data: the original-ecGEM, DL-ecGEM and posterior-mean-ecGEM are shown. Four species with absolute proteome data were evaluated. Original-ecGEMs were constructed following the pipeline to extract k_{cat} profiles from BRENDA and SABIO-RK; DL-ecGEMs were constructed from DLKcat-predicted k_{cat} profiles; and posterior-mean-ecGEMs were parameterized with mean k_{cat} values from 100 posterior datasets after the Bayesian training process. Culture conditions for the labels on the *x* axis of those proteome datasets can be found in Supplementary Table 7, and the collected proteome datasets are available in the GitHub repository. sce, *S. cerevisiae*; kla, *Kluyveromyces lactis*; kmx, *Kluyveromyces marxianus*; yli, *Y. lipolytica*. DL, deep learning-predicted. In the violin plot (**a**, **b** and **c**), white shaded box limits stands for the upper and lower quartiles; the central line limits stands for the 1.5× interquartile range.

deep learning-predicted k_{cat} process proved to be a more comprehensive but still practical alternative to matching in vitro k_{cat} values from the BRENDA[4] and SABIO-RK[5] databases, as is common in original-ecGEM reconstruction pipelines such as the GECKO and MOMENT[2,8,47]. By not depending on EC number annotation, DLKcat is furthermore able to predict isozyme-specific k_{cat} values, while the use of SMILES (matching via the PubChem[48] or MetaNetX[49] databases) avoids the issues of ununified substrate naming between the GEM and BRENDA that original-ecGEM reconstruction pipelines can experience. The DL-ecGEMs can subsequently be adjusted to existing experimental growth data through a Bayesian approach that yields posterior-mean-ecGEMs with physiologically relevant solution spaces. Combined, the current DLKcat-based pipeline is therefore applicable to ecGEM reconstruction for virtually any organism for which a protein sequence FASTA file and a basic GEM is available. Our pipeline hereby improves applicability, and it even improves the number of reactions with enzymatic constraints in comparison with original-ecGEMs that have previously been constr ucted[2,8–12,50].

Even though the DLKcat-based pipeline yields ecGEMs with superior performance over original-ecGEMs, various challenges remain. For example, while our deep learning model can distinguish alternative from randomly chosen substrates for promiscuous enzymes (Fig. 2c), it still predicts a level of kinetic activity towards random substrates that is likely too high. This behaviour can be explained by the limited availability of negative data: cases where an enzyme–substrate pair did not result in catalysis. Increased reporting of negative datasets, where non-detected activity for enzyme–substrate pairs are reported and collected by enzyme databases, could enhance future deep learning models in terms of defining true negatives[46]. In addition, DLKcat did not consider the effect of environmental factors such as pH and temperature, but combining DLKcat with other emerging machine learning tools, such as for enzyme optimal temperature prediction, would enable future investigation on the impact of environmental parameters on enzyme activities[32].

Another challenge relates to reactions involving multiple substrates and those catalysed by heteromeric enzyme complexes. The multiple substrate SMILES and protein sequences that can be defined for such reactions can all function with DLKcat, thereby yielding multiple predicted k_{cat} values for one reaction. We currently select the maximum k_{cat} values in those cases, but it would be favourable to devise an approach that can predict one k_{cat} value for each multi-substrate and/or heteromeric enzyme.

In addition, DLKcat-derived DL-ecGEMs and posterior-mean-ecGEMs inherit limitations from basic (non-ec) GEMs, where the steady-state assumption that is central to constraint-based modelling allows one to determine metabolic fluxes but does not readily consider regulatory behaviours. While ecGEMs drastically reduce the solution space of constraint-based models to cellular feasible capacities, k_{cat} is not the only kinetic parameter that determines reaction rate, as for example, affinity constants play influential roles. However, as constraint-based models cannot predict internal metabolite concentrations, it is currently not feasible to readily consider the influence of those parameters. Nonetheless, k_{cat} values are also important parameters in other resource allocation models such as proteome-constrained GEMs[51–53] and metabolism/macromolecular-expression models[7,54,55]. Despite improved predictions and more applications, how to define k_{cat} values has also remained a challenge in the reconstruction of those models. Such resource allocation models and ecGEMs share the assertion that cells need to allocate their limited proteome to different pathways to achieve faster growth or better fitness, while the proteome cost for each reaction is similarly defined by the flux and the kinetic rate of the enzyme. Deep learning-predicted k_{cat} values for the metabolic parts of those models can therefore improve their quality and performance, although other challenging kinetic parameters, for example, ribosomal catalytic rates, to be determined in those model formulations cannot be obtained from DLKcat. In addition, model formulations that particularly focus on describing enzyme kinetics[56] could benefit from deep learning-predicted k_{cat} values, so that our DLKcat approach can find a broad application in the modelling field.

In conclusion, we showed that DLKcat yields realistic k_{cat} values that can be used to direct future genetic engineering, understand

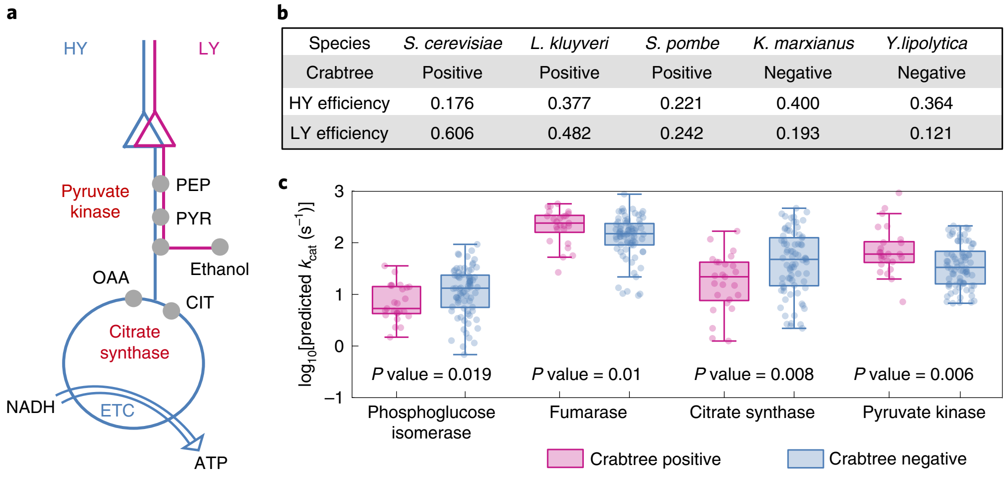

Species	*S. cerevisiae*	*L. kluyveri*	*S. pombe*	*K. marxianus*	*Y.lipolytica*
Crabtree	Positive	Positive	Positive	Negative	Negative
HY efficiency	0.176	0.377	0.221	0.400	0.364
LY efficiency	0.606	0.482	0.242	0.193	0.121

Fig. 6 | Explanation of the Crabtree effect by energy metabolism. a, HY and LY pathway definitions. PEP, phosphoenolpyruvate; PYR, pyruvate; OAA, oxaloacetate; CIT, citrate; ETC, electron transport chain. **b**, Model-inferred protein efficiency of energy metabolism in several common yeast species. Protein efficiency is the ATP produced per protein mass per unit time, in units of millimoles ATP per grams protein per hour. *L. kluyveri*, *Lachancea kluyveri*. **c**, Enzymes with significantly different k_{cat} values between Crabtree positive and negative species. A two-sided Wilcoxon rank sum test was used to calculate *P* values. Crabtree positive species ($n=25$) and Crabtree negative species ($n=77$) were examined in this analysis. In the box plot, the central band represents the median value, the box represents the upper and lower quartiles and the whiskers extend up to 1.5 times the interquartile range beyond the box range.

enzyme evolution and reconstruct ecGEMs to predict metabolic fluxes and phenotypes. Besides that, we envision many other possible uses of this deep learning-based k_{cat} prediction tool, such as a tool in genome mining and Genome-Wide Association Studies analysis. The developed automatic Bayesian ecGEM reconstruction pipeline will be instrumental for further use in ecGEM reconstruction, for omics data incorporation and analysis.

Methods

Dataset preparation for deep learning model development. The dataset used for deep learning model construction was extracted from the BRENDA[4] and SABIO-RK databases[5] on 10 July 2020 by customized scripts via application programming interface. We generated a comprehensive dataset including the substrate name, organism information, EC number, protein identifier (UniProt ID), enzyme type and k_{cat} values. As the overall majority of k_{cat} values reported in BRENDA and SABIO-RK do not specify their assay conditions, such as pH and temperature, we decided not to include the features in order to maintain the training dataset size and variety. In addition, substrate SMILES, a string notation to represent the substrate structure, was extracted using substrate name to query the PubChem compound database[48], which is the largest database of chemical compound information and is easy to access[57]. As different substrates usually have various synonyms in different databases and GEMs, we used a customized Python-based script to ensure that the same canonical SMILES information could be output for the same substrates with various synonyms, which is essential to help filter redundant entries obtained from different databases. Several rounds of data cleaning were performed to ensure quality (Supplementary Fig. 2). Protein sequences were queried with two methods: for entries with UniProt ID information, the amino acid sequences could be obtained via the application programming interface of the UniProt[58] with the help of Biopython v.1.78 (https://biopython.org/); and for entries without UniProt ID, the amino acid sequences were acquired from the UniProt[58] and the BRENDA[4] databases based on their EC number and organism information. After that, the sequences of those entries with wild-type enzymes were mapped directly, and the sequences of those entries with mutated enzymes were changed according to the mutated sites. Finally, the remaining entries formed the high-quality dataset for deep learning model construction. Detailed numbers for the data cleaning can be found in Supplementary Fig. 2.

Construction of the deep learning pipeline. In this work, we developed an end-to-end learning approach for in vitro k_{cat} value prediction by combining a GNN for substrates and a CNN for proteins. The integration of GNN and CNN can be naturally used to handle pairs of data with different structures, that is, molecular graphs and protein sequences. In this approach, substrates are represented as molecular graphs where the vertices are atoms and the edges are chemical bonds, while proteins are represented as sequences in which the characters are amino acids.

For substrates, there are just a few types of chemical atoms (for example, carbon and hydrogen) and chemical bonds (for example, single bond and double bond). To obtain more learning parameters, we employed *r*-radius subgraphs to get the vector representations, which are induced by the neighbouring vertices and edges within radius *r* from a vertex[59]. First, substrate SMILES information was converted to a molecular graph using RDKit v.2020.09.1 (https://www.rdkit.org). Given a substrate graph, the GNN can update each atom vector and its neighbouring atom vectors transformed by the neural network via a nonlinear function, for example, ReLU (ref. [60]). In addition, two transitions were developed in the GNN, including vertex transitions and edge transitions. The aim of transitions is to ensure that the local information of vertices and edges is propagated in the graph by iterating the process and summing neighbouring embeddings. The final output of the GNN is a set of real-valued molecular vector representations for substrates.

Similarly, by using the CNN to scan protein sequences, we can obtain low-dimensional vector representations for protein sequences transformed by the neural network via a nonlinear function, for example, ReLU. To apply the CNN to proteins, we defined ‘words’ in protein sequence and split a protein sequence into an overlapping *n*-gram ($n=1, 2, 3$) of amino acids[61]. In this work, to avoid low-frequency words in the learning representations, a relatively smaller *n*-gram number of 1, 2 or 3 was set. Then, we translated protein sequences into various word embeddings. Following this, the CNN used a filter function, shown in equation (1), to compute the hidden vectors from the input word embeddings and weight matrix. After that, we obtained a set of hidden vectors for these split subsequences based on *n*-gram amino acid splitting.

$$\mathbf{c}_i^{(t)} = f\left(W_{\text{conv}}\mathbf{c}_i^{(t-1)} + \mathbf{b}_{\text{conv}}\right) \qquad (1)$$

where *f* is a nonlinear activation function (for example, ReLU); W_{conv} is the weight matrix and $\mathbf{b}_{\text{conv}}$ is the bias vector; *i* and *t* are the serial numbers of a set of hidden vectors; and $\mathbf{c}_i^{(t)}$ and $\mathbf{c}_i^{(t-1)}$ are the hidden vectors for the protein sequence.

Also, other important parameters of the neural networks (CNN and GNN) were set as follows: number of convolutional layers in CNN, 2, 3 or 4; number of time steps in GNN, 2, 3 or 4; window size, 11 (fixed); *r*-radius, 0, 1 or 2; and vector dimensionality, 5, 10 or 20. These different settings were explored based on the coefficient of determination (R^2) in equation (2) during the hyperparameter tuning to find which hyperparameter is better for improving the deep learning performance. The R^2 was calculated by scikit-learn v.0.23.2 (https://scikit-learn.org/stable/). And finally, we used the optimal hyperparameters to train our deep learning model.

$$R^2 = 1 - \frac{\sum_{i=1}^{n}(y_{ie} - y_{ip})^2}{\sum_{i=1}^{n}(y_{ie} - \bar{y})^2} \qquad (2)$$

where y_{ip} is the predicted k_{cat} value, y_{ie} is the experimental k_{cat} value, $\bar{y}$ is the average of the experimental k_{cat} values and *n* is the total number of items in the dataset (validation dataset or test dataset).

After the acquisition of the substrate molecular vector representations and the protein sequence vector representations, we concatenated them together along with an output vector (k_{cat} value) to train the deep learning model using the neural attention mechanism[59]. During the training process, all the datasets were shuffled at the first step, and then were randomly split into a training dataset, validation dataset and test dataset at the ratio of 80%:10%:10%. Given a set of substrate–protein pairs and the k_{cat} values in the training dataset, the aim of the training process is to minimize its loss function. The best model was chosen according to the minimal r.m.s.e., shown in equation (3), on the validation dataset with the least spread between the training dataset and validation dataset. For building and training models, the PyTorch v.1.4.0 software package was used and accessed using the Python package v.3.7.6 interface under CUDA/10.1.243. In addition, data processing was mainly implemented by NumPy v.1.20.2, SciPy v.1.5.2 and pandas v.1.1.3. Data visualization was implemented by Matplotlib v.3.3.2 and seaborn v.0.11.0.

$$\text{r.m.s.e.} = \sqrt{\frac{1}{n}\sum_{i=1}^{n}(y_{ip} - y_{ie})^2} \tag{3}$$

where y_{ip} is the predicted k_{cat} value, y_{ie} is the experimental k_{cat} value and n is the total number of items in the dataset (validation dataset or test dataset).

Enzyme promiscuity analysis based on deep learning model. For enzyme promiscuity, we explored whether the deep learning model can identify substrate preference for promiscuous enzymes. For each promiscuous enzyme, we defined that the substrate with the highest k_{cat} value was considered as the preferred substrate, while those with k_{cat} values less than the maximum value were classified as alternative substrates. Random substrates were randomly chosen from the compound dataset in our training data, except for the documented substrates and products for the tested enzyme. By using the deep learning model, we further predicted and compared the k_{cat} values for the preferred, alternative and random substrates on various promiscuous enzymes. In order to identify high-quality promiscuous enzymes, entries with an experimentally measured k_{cat} value less than −2 (s^{-1}) in a $\log_{10}$ scale were excluded in this analysis.

Validation of deep learning-based k_{cat} values. According to the classification of metabolic pathways, metabolic contexts were mainly divided into four different subsystems: (1) primary metabolism (carbohydrate and energy), involving the main carbon and energy metabolism, for example, glycolysis/gluconeogenesis, TCA cycle, pentose phosphate pathway, and so on; (2) primary metabolism (amino acids, fatty acids and nucleotides); (3) intermediate metabolism, related to the biosynthesis and degradation of cellular components, such as coenzymes and cofactors; and (4) secondary metabolism[6]. To explore the metabolic subsystems for all of the wild-type enzymes in the experimental dataset, the module in the KEGG database[62] was used to assign metabolic pathways for enzyme–substrate pairs by linking the detailed metabolic pathway in the KEGG application programming interface with the EC number annotated in each enzyme–substrate pair. Detailed classification can be found in Supplementary Table 1. Using the trained deep learning model, the predicted k_{cat} values were generated for all the enzyme–substrate pairs.

Interpretation of the reasoning of deep learning. To interpret which subsequences or residue sites are more important for the substrate, the neural attention mechanism was employed by assigning attention weights to the subsequences[27]. A higher attention weight of one residue means that that residue is more important for the enzyme activity towards the specific substrate. Such attention weights were modelled based on the output of the neural network. The mathematical equations for the neural attention mechanism are shown as follows:

$$\mathbf{C} = \left\{\mathbf{c}_1^{(t)}, \mathbf{c}_2^{(t)}, \mathbf{c}_3^{(t)}, \ldots, \mathbf{c}_n^{(t)}\right\} \tag{4}$$

$$h_{\text{substrate}} = f(W_{\text{inter}}\mathbf{y}_{\text{substrate}} + \mathbf{b}) \tag{5}$$

$$h_i = f(W_{\text{inter}}\mathbf{c}_i + \mathbf{b}) \tag{6}$$

$$\alpha_i = \sigma\left(h_{\text{substrate}}^{\text{T}} h_i\right) \tag{7}$$

where $\mathbf{C}$ is a set of hidden vectors for the protein sequence, $\mathbf{c}_1^{(t)}$ to $\mathbf{c}_n^{(t)}$ are the sub-hidden vectors for the split subsequences, $\mathbf{y}_{\text{substrate}}$ is the substrate molecular vector, W_{inter} and $\mathbf{b}$ are the weight matrix and the bias vector in the neural network, respectively, f is a nonlinear activation function (for example, ReLU), α_i is the final attention weight value, σ is the element-wise sigmoid function, and T is the transpose function.

A defined protein could be split into overlapping n-gram amino acids and calculated as a set of hidden vectors in equation (4). Given a substrate molecular vector $\mathbf{y}_{\text{substrate}}$ and a set of protein hidden vectors, the substrate embeddings ($h_{\text{substrate}}$) and subsequence embeddings (h_i) could be output based on the neural network, as shown in equations (5) and (6). By considering the embeddings of $\mathbf{y}_{\text{substrate}}$, the attention weight value for each subsequence was accessible in equation (7), which represents the importance signals of the protein subsequence towards the enzyme activity for a certain substrate.

Prediction of k_{cat} values for 343 yeast/fungi species. The GEMs of 343 yeast/fungi species were automatically reconstructed in our previous paper[14] from a yeast/fungi 'pan-GEM', which was derived from the well-curated Yeast8 of *S. cerevisiae* combined with the pan-genome annotation. For each model, all reversible enzymatic reactions were split into forward and backward reactions. Reactions catalysed by isoenzymes were also split into multiple reactions with one enzyme complex for each reaction. Substrates were extracted from the model and mapped to the MetaNetX database to get SMILES information using annotated MetaNet identifiers (IDs) for metabolites[49]. Protein IDs for the enzymes were from the model grRules. Protein sequences were queried by the protein ID in the protein FASTA file for each species. Reaction IDs, substrate names, substrate SMILES information and protein IDs were combined as the input file for the deep learning k_{cat} prediction model.

Analysis of k_{cat} values and dN/dS for yeast/fungi species. In a previous study, the genomes of 343 yeast/fungi species combined with comprehensive genome annotations were publicly available[63]. The gene-level dN/dS of gene sequences for pairs of orthologous genes from the 343 species were calculated with yn00 from PAML v.4.7 (ref. [64]). For this computational framework, the input is the single-copy ortholog groups, and the output is the gene-level dN/dS values extracted from the PAML output files. By mapping the predicted k_{cat} values with the gene-level dN/dS values via the bridge of protein ID, a global analysis was performed between the k_{cat} values and the dN/dS values for 343 yeast/fungi species across the out-group (11 fungal species) together with 12 major clades divided by the genus-level phylogeny for 332 yeast species.

ecGEM reconstruction. Besides the constraints in basic (non-ec) GEM, shown in equations (8) and (9), ecGEMs are reconstructed by adding enzymatic constraints, shown in equations (10) and (11).

$$\text{Subject to } S \times v = 0 \tag{8}$$

in which S is the stoichiometry matrix and v is the flux vector. This equation is the representative of the steady-state assumption of the metabolic model to constrain the mass balance.

$$\text{lb}_j \leq v_j \leq \text{ub}_j \tag{9}$$

in which lb and ub are the lower bound and upper bound of the rate for the reaction j.

$$v_j \leq k_{\text{cat}}^{i,j} \times [E_i] \tag{10}$$

where v_j stands for the metabolic flux (mmol gDW^{-1} h^{-1}; gDW, gram dry weight) of the reaction j; $[E_i]$ stands for the enzyme concentration for the enzyme i that catalyses reaction j; and $k_{\text{cat}}^{i,j}$ is the catalytic turnover number for the enzyme catalysing reaction j. This constraint is applied to all enzymatic reactions with available k_{cat} values. Additionally, we added reactions to draw protein mass from the total protein pool to each enzyme, therefore, a mass balance constraint was proposed as:

$$\sum [E_i] \leq \theta \times \text{total protein abundance} \tag{11}$$

where θ is the fraction of metabolic protein in the total protein content of the cell. This equation means that the sum enzyme usage should be lower or equal to the total metabolic protein abundance.

To compare the different k_{cat} value assignment approaches, we built ecGEMs parameterized with three types of k_{cat} values: original-ecGEMs, DL-ecGEMs and posterior-mean-ecGEMs.

Original-ecGEM reconstruction queried k_{cat} values from the BRENDA database by matching the EC number, a method that relies heavily on the database EC number annotation for the specific species[2,8]. Since more than 200 out of 343 yeast/fungi species are not annotated in UniProt[58] and KEGG[62], EC numbers for orthologs annotated in *S. cerevisiae* were borrowed to facilitate the original-ecGEM reconstruction process for all these 343 species. The k_{cat} extraction process used the criteria from process 13 in the reconstruction methods of the reference[47].

DL-ecGEM reconstruction extracted all k_{cat} values from the deep learning predicted file. To assign a k_{cat} value for each metabolic reaction, we followed these criteria: If the in vitro k_{cat} measurement with matched substrate and enzyme was available, then the measured in vitro k_{cat} values were used rather than the k_{cat} prediction. This pipeline also accepted the user's input for the k_{cat} values. For enzymes with no k_{cat} measurement, predicted k_{cat} values were used after the following steps: k_{cat} values predicted for currency metabolites such as H_2O and H^+ were excluded; if there were multiple substrates in the reaction, maximum values among the substrates were kept; and if multiple subunits existed in the enzyme complex, we used the maximum value among all subunits to represent the k_{cat} for the complex. Subunit protein stoichiometry information was multiplied before comparison. We assumed the same enzyme complex stoichiometry information for yeast species as that of *S. cerevisiae*, which is collected from the Protein Data Bank in Europe database (https://www.ebi.ac.uk/pdbe/) as well as the Complex Portal (www.ebi.ac.uk/complexportal).

Posterior-mean-ecGEM reconstruction was parameterized by mean k_{cat} values from accepted posterior distribution. The k_{cat} values in the DL-ecGEMs combined with the r.m.s.e. (which is 1 in the $\log_{10}$ scale) of the k_{cat} prediction were used as mean values and variance to make the prior distribution. Each k_{cat} value was described with a log normal distribution $N(k_{cat}^{i}, 1)$. This prior iteratively morphs into a posterior through multiple generations[32]. For each generation, we sampled 126 k_{cat} datasets within the distribution; 100 among those 126 datasets with a smaller distance (see next section for the SMC-ABC distance calculation) between the phenotype measurements and predictions, which can better represent the phenotype, were kept to make the distribution for the next generation. Until the distance was lower than the cut-off (r.m.s.e. for phenotype prediction of 1), we accepted the final distribution as the posterior distribution[32].

SMC-ABC distance function. Experimental growth data and related exchange rates in batch and chemostat conditions were collected for the yeast/fungi species, which are available in Supplementary Table 5. The distance function was designed as the r.m.s.e. between the simulated and experimental phenotypes. To have a metric for the variance of phenotype prediction of both flux and maximum growth potential, r.m.s.e. was designed in two parts (each part may contain multiple measurement entries such as growth with a different medium). The first part addressed flux prediction. This part checks whether the model predicts similar fluxes when the carbon uptake rate is constrained, as experimentally measured. In this part, all data points for the species are used, and all measured exo-metabolite exchange fluxes are used for comparison. The second part addresses the prediction of the maximum growth rate potential. This part checks the maximum growth rate of the model prediction against the experimental measurement for one species on a certain experimentally tested medium. In this part, only the batch condition with maximum growth rate measurement was tested. No carbon uptake rate or other exchange rate was constrained in the model. Growth maximization was set as the objective function. After simulation, only the maximum growth rate and the carbon uptake rates were used for comparison with measurement.

After running the above two parts of the simulations, the r.m.s.e. for each part can be calculated. All measured and simulated rates were normalized by multiplying the carbon numbers of the corresponding metabolites before calculation of r.m.s.e. The carbon number for biomass is 41 (the mean value for the molecular weight of 1 carbon moles (Cmol) biomass of yeast is ~24.42 g (ref. [65]); the biomass equals 1,000 mg). Note that if the substrate or by-product does not contain any carbon, such as O_2, then the normalizing number is 1. Then the average r.m.s.e. of both simulations was used to represent the distance. The SMC-ABC search stopped once the r.m.s.e. reached the accepted value or reached the maximum generation. The accepted value for the distance was set to be lower than 1, and the maximum generation was set to be 100.

Simulations with ecGEMs. We performed different kinds of simulations using the ecGEMs, including simulations of growth and protein abundance. Different media and growth conditions were set to match the experiment measurement conditions, for example, using xylose as the carbon source or anaerobic conditions. Since there are no measured total protein abundances in the biomass for all yeast/fungi species, we used the protein content mass to serve as the default total protein abundance for each species and used a factor of 0.5 to serve as the ratio of the metabolic protein to the total protein.

As for the protein abundance simulation, the medium was set to match the experimental condition as mentioned above. For the chemostat condition, the growth rate was fixed as the dilution rate, and the carbon source uptake rate was minimized, which is a normal set-up for the simulation of the chemostat condition. For the batch condition, the growth rate maximization was used as the objective. Then, the simulated protein abundances, which can be extracted from the fluxes, were compared with those in collected proteome datasets. The MATLAB (2019b), COBRA (v.3.2)[66], RAVEN (v.2.4)[67] and libSBML (v.5.17.0) toolboxes were used in the process with solver IBM ILOG CPLEX optimizer. Violinplot-Matlab (https://github.com/bastibe/Violinplot-Matlab) was used for the visualization of violin plots.

Statistical tests for Bayesian approach. Sampled prior and posterior k_{cat} datasets were compared for the difference in the mean values and the variance. Welch's *t*-test was used to test the significance for the mean values, while a one-tailed *F*-test was used for the reduced variances. The cut-off for the significance was set to 0.01 for the adjusted *P* value corrected by the Šidák method. PVAL_ADJUST (https://github.com/nunofachada/pval_adjust) was used in the analysis.

Proteome data processing. We normalized the collected relative proteome datasets using the identical condition of the absolute proteome data from the literature following the same method as in ref. [68]. The reference absolute datasets for those relative proteome datasets were documented in the collected file in the GitHub repository.

Calculation of protein cost and efficiency. To calculate the protein cost of the HY pathway, the glucose uptake rate was fixed at 1 mmol gDW^{-1} h^{-1}, and the non-growth associated maintenance energy (NGAM) reaction was maximized. The total protein pool reaction was then minimized by fixing the NGAM reaction at the maximized value. The minimized flux through the total protein pool reaction is the protein cost of the HY pathway for converting one glucose to ATP. As for the protein cost calculation of the LY pathway, the glucose uptake rate was fixed at 1 mmol gDW^{-1} h^{-1}, and ethanol production was maximized. Then the ethanol exchange rate was fixed at the maximized value, and NGAM was maximized. After that, NGAM was also fixed at the maximized value, and the total protein pool was minimized to calculate the protein cost for the LY pathway. We also examined the flux distribution to ensure that other energy-producing pathways were all inactive during this simulation. Protein efficiency is defined as the protein cost for producing one flux ATP in each pathway.

Reporting summary. Further information on research design is available in the Nature Research Reporting Summary linked to this article.

Data availability

Protein sequence FASTA files, deep learning predicted k_{cat} values, GEMs, original-ecGEMs, DL-ecGEMs and posterior-mean-ecGEMs for 343 yeast/fungi species are available as a supplementary dataset on Zenodo: https://doi.org/10.5281/zenodo.6438262. Collected proteome data are available in the GitHub repository: https://github.com/SysBioChalmers/DLKcat/tree/master/BayesianApporach/Data/Proteome_ref.xlsx. All other collected datasets such as the training dataset and the deep learning model are available in the GitHub repository: https://github.com/SysBioChalmers/DLKcat. Databases including BRENDA (https://www.brenda-enzymes.org), SABIO-RK (http://sabiork.h-its.org/), UniProt database (https://www.uniprot.org/) and PubChem (https://pubchem.ncbi.nlm.nih.gov) were used in the DLKcat model construction. KEGG (http://www.kegg.jp/) was used in the evaluation of the DLKcat performance. Databases including the MetaNetX database (https://www.metanetx.org/), the Protein Data Bank in Europe database (https://www.ebi.ac.uk/pdbe/) and the Complex Portal (https://www.ebi.ac.uk/complexportal) were used in the ecGEM reconstruction. The authors declare that all data supporting the findings and for reproducing all figures of this study are available within the paper and its Supplementary Information. Source data are provided with this paper.

Code availability

To facilitate further usage, we provide all codes and detailed instruction in the GitHub repository: https://github.com/SysBioChalmers/DLKcat. A user-friendly example for k_{cat} prediction is also included in the repository.

Received: 11 August 2021; Accepted: 2 May 2022;
Published online: 16 June 2022

References

1. Chen, Y. & Nielsen, J. Energy metabolism controls phenotypes by protein efficiency and allocation. *Proc. Natl Acad. Sci. USA* **116**, 17592–17597 (2019).
2. Sánchez, B. J. et al. Improving the phenotype predictions of a yeast genome-scale metabolic model by incorporating enzymatic constraints. *Mol. Syst. Biol.* **13**, 935 (2017).
3. Klumpp, S., Scott, M., Pedersen, S. & Hwa, T. Molecular crowding limits translation and cell growth. *Proc. Natl Acad. Sci. USA* **110**, 16754–16759 (2013).
4. Schomburg, I. et al. The BRENDA enzyme information system–from a database to an expert system. *J. Biotechnol.* **261**, 194–206 (2017).
5. Wittig, U., Rey, M., Weidemann, A., Kania, R. & Müller, W. SABIO-RK: an updated resource for manually curated biochemical reaction kinetics. *Nucleic Acids Res.* **46**, D656–D660 (2018).
6. Bar-Even, A. et al. The moderately efficient enzyme: evolutionary and physicochemical trends shaping enzyme parameters. *Biochemistry* **50**, 4402–4410 (2011).
7. Chen, Y. & Nielsen, J. Mathematical modelling of proteome constraints within metabolism. *Curr. Opin. Syst. Biol.* **25**, 50–56 (2021).
8. Bekiaris, P. S. & Klamt, S. Automatic construction of metabolic models with enzyme constraints. *BMC Bioinf.* **21**, 19 (2020).
9. Ye, C. et al. Improving lysine production through construction of an *Escherichia coli* enzyme-constrained model. *Biotechnol. Bioeng.* **117**, 3533–3544 (2020).
10. Domenzain, I. et al. Reconstruction of a catalogue of genome-scale metabolic models with enzymatic constraints using GECKO 2.0. Preprint at *bioRxiv* https://doi.org/10.1101/2021.03.05.433259 (2021).
11. Yeo, H. C., Hong, J., Lakshmanan, M. & Lee, D.-Y. Enzyme capacity-based genome scale modelling of CHO cells. *Metab. Eng.* **60**, 138–147 (2020).

12. Robinson, J. L. et al. An atlas of human metabolism. *Sci. Signal.* **13**, eaaz1482 (2020).
13. Nilsson, A., Nielsen, J. & Palsson, B. O. Metabolic models of protein allocation call for the kinetome. *Cell Syst.* **5**, 538–541 (2017).
14. Lu, H. et al. Yeast metabolic innovations emerged via expanded metabolic network and gene positive selection. *Mol. Syst. Biol.* **17**, e10427 (2021).
15. Davidi, D. & Milo, R. Lessons on enzyme kinetics from quantitative proteomics. *Curr. Opin. Biotechnol.* **46**, 81–89 (2017).
16. Heckmann, D. et al. Machine learning applied to enzyme turnover numbers reveals protein structural correlates and improves metabolic models. *Nat. Commun.* **9**, 5252 (2018).
17. Kitchin, J. R. Machine learning in catalysis. *Nat. Catal.* **1**, 230–232 (2018).
18. Shrivastava, A. D. & Kell, D. B. FragNet, a contrastive learning-based transformer model for clustering, interpreting, visualizing, and navigating chemical space. *Molecules* **26**, 2065 (2021).
19. Zrimec, J. et al. Deep learning suggests that gene expression is encoded in all parts of a co-evolving interacting gene regulatory structure. *Nat. Commun.* **11**, 6141 (2020).
20. Kroll, A., Engqvist, M. K. M., Heckmann, D. & Lercher, M. J. Deep learning allows genome-scale prediction of Michaelis constants from structural features. *PLoS Biol.* **19**, e3001402 (2021).
21. Ryu, J. Y., Kim, H. U. & Lee, S. Y. Deep learning enables high-quality and high-throughput prediction of enzyme commission numbers. *Proc. Natl Acad. Sci. USA* **116**, 13996–14001 (2019).
22. Notebaart, R. A., Kintses, B., Feist, A. M. & Papp, B. Underground metabolism: network-level perspective and biotechnological potential. *Curr. Opin. Biotechnol.* **49**, 108–114 (2018).
23. Kuznetsova, E. et al. Genome-wide analysis of substrate specificities of the *Escherichia coli* haloacid dehalogenase-like phosphatase family. *J. Biol. Chem.* **281**, 36149–36161 (2006).
24. Notebaart, R. A. et al. Network-level architecture and the evolutionary potential of underground metabolism. *Proc. Natl Acad. Sci. USA* **111**, 11762–11767 (2014).
25. Yep, A., Kenyon, G. L. & McLeish, M. J. Saturation mutagenesis of putative catalytic residues of benzoylformate decarboxylase provides a challenge to the accepted mechanism. *Proc. Natl Acad. Sci. USA* **105**, 5733–5738 (2008).
26. Lin, Y.-H. T., Huang, C. L. V., Ho, C., Shatsky, M. & Kirsch, J. F. A general method to predict the effect of single amino acid substitutions on enzyme catalytic activity. Preprint at *bioRxiv* https://doi.org/10.1101/236265 (2017).
27. Bahdanau, D., Cho, K. & Bengio, Y. Neural machine translation by jointly learning to align and translate. Preprint at https://doi.org/10.48550/arXiv.1409.0473 (2014).
28. Erion, M. D. et al. Purine nucleoside phosphorylase. 1. Structure-function studies. *Biochemistry* **36**, 11725–11734 (1997).
29. Nam, H. et al. Network context and selection in the evolution to enzyme specificity. *Science* **337**, 1101–1104 (2012).
30. Kryazhimskiy, S. & Plotkin, J. B. The population genetics of dN/dS. *PLoS Genet.* **4**, e1000304 (2008).
31. Ringe, D. & Petsko, G. A. Biochemistry. How enzymes work. *Science* **320**, 1428–1429 (2008).
32. Li, G. et al. Bayesian genome scale modelling identifies thermal determinants of yeast metabolism. *Nat. Commun.* **12**, 190 (2021).
33. Van Hoek, P. I. M., Van Dijken, J. P. & Pronk, J. T. Effect of specific growth rate on fermentative capacity of baker's yeast. *Appl. Environ. Microbiol.* **64**, 4226–4233 (1998).
34. Pfeiffer, T. & Morley, A. An evolutionary perspective on the Crabtree effect. *Front. Mol. Biosci.* **1**, 17 (2014).
35. de Alteriis, E., Cartenì, F., Parascandola, P., Serpa, J. & Mazzoleni, S. Revisiting the Crabtree/Warburg effect in a dynamic perspective: a fitness advantage against sugar-induced cell death. *Cell Cycle* **17**, 688–701 (2018).
36. Ata, Ö. et al. A single Gal4-like transcription factor activates the Crabtree effect in *Komagataella phaffii*. *Nat. Commun.* **9**, 4911 (2018).
37. Kamrad, S. et al. Pyruvate kinase variant of fission yeast tunes carbon metabolism, cell regulation, growth and stress resistance. *Mol. Syst. Biol.* **16**, e9270 (2020).
38. Krebs, H. A. Rate control of the tricarboxylic acid cycle. *Adv. Enzym. Regul.* **8**, 335–353 (1970).
39. Christen, S. & Sauer, U. Intracellular characterization of aerobic glucose metabolism in seven yeast species by ^{13}C flux analysis and metabolomics. *FEMS Yeast Res.* **11**, 263–272 (2011).
40. Blank, L. M., Lehmbeck, F. & Sauer, U. Metabolic-flux and network analysis in fourteen hemiascomycetous yeasts. *FEMS Yeast Res.* **5**, 545–558 (2005).
41. Chen, K. & Arnold, F. H. Engineering new catalytic activities in enzymes. *Nat. Catal.* **3**, 203–213 (2020).
42. Markel, U. et al. Advances in ultrahigh-throughput screening for directed enzyme evolution. *Chem. Soc. Rev.* **49**, 233–262 (2020).
43. Loeb, D. D. et al. Complete mutagenesis of the HIV-1 protease. *Nature* **340**, 397–400 (1989).
44. Lee, J. & Goodey, N. M. Catalytic contributions from remote regions of enzyme structure. *Chem. Rev.* **111**, 7595–7624 (2011).
45. Tong, H., Küken, A., Razaghi-Moghadam, Z. & Nikoloski, Z. Characterization of effects of genetic variants via genome-scale metabolic modelling. *Cell. Mol. Life Sci.* **78**, 5123–5138 (2021).
46. Mazurenko, S., Prokop, Z. & Damborsky, J. Machine learning in enzyme engineering. *ACS Catal.* **10**, 1210–1223 (2019).
47. Chen, Y., Li, F., Mao, J., Chen, Y. & Nielsen, J. Yeast optimizes metal utilization based on metabolic network and enzyme kinetics. *Proc. Natl. Acad. Sci. USA* **118**, e2020154118 (2021).
48. Kim, S. et al. PubChem 2019 update: improved access to chemical data. *Nucleic Acids Res.* **47**, D1102–D1109 (2019).
49. Moretti, S., Tran, V. D. T., Mehl, F., Ibberson, M. & Pagni, M. MetaNetX/MNXref: unified namespace for metabolites and biochemical reactions in the context of metabolic models. *Nucleic Acids Res.* **49**, D570–D574 (2021).
50. Adadi, R., Volkmer, B., Milo, R., Heinemann, M. & Shlomi, T. Prediction of microbial growth rate versus biomass yield by a metabolic network with kinetic parameters. *PLoS Comput. Biol.* **8**, e1002575 (2012).
51. Chen, Y. et al. Proteome constraints reveal targets for improving microbial fitness in nutrient-rich environments. *Mol. Syst. Biol.* **17**, e10093 (2021).
52. Elsemman, I. E. et al. Whole-cell modeling in yeast predicts compartment-specific proteome constraints that drive metabolic strategies. *Nat. Commun.* **13**, 801 (2022).
53. Li, F. et al. Genome scale modeling of the protein secretory pathway reveals novel targets for improved recombinant protein production in yeast. Preprint at *bioRxiv* https://doi.org/10.1101/2021.10.16.464630 (2021).
54. Oftadeh, O. et al. A genome-scale metabolic model of *Saccharomyces cerevisiae* that integrates expression constraints and reaction thermodynamics. *Nat. Commun.* **12**, 4790 (2021).
55. Lloyd, C. J. et al. COBRAme: a computational framework for genome-scale models of metabolism and gene expression. *PLoS Comput. Biol.* https://doi.org/10.1371/journal.pcbi.1006302 (2018).
56. Islam, M. M., Schroeder, W. L. & Saha, R. Kinetic modeling of metabolism: present and future. *Curr. Opin. Syst. Biol.* **26**, 72–78 (2021).
57. Chen, F., Yuan, L., Ding, S., Tian, Y. & Hu, Q.-N. Data-driven rational biosynthesis design: from molecules to cell factories. *Brief. Bioinform.* **21**, 1238–1248 (2020).
58. The UniProt Consortium. UniProt: the universal protein knowledgebase. *Nucleic Acids Res.* **45**, D158–D169 (2017).
59. Tsubaki, M., Tomii, K. & Sese, J. Compound-protein interaction prediction with end-to-end learning of neural networks for graphs and sequences. *Bioinformatics* **35**, 309–318 (2019).
60. LeCun, Y., Bengio, Y. & Hinton, G. Deep learning. *Nature* **521**, 436–444 (2015).
61. Dong, Q.-W., Wang, X.-L. & Lin, L. Application of latent semantic analysis to protein remote homology detection. *Bioinformatics* **22**, 285–290 (2006).
62. Kanehisa, M., Furumichi, M., Tanabe, M., Sato, Y. & Morishima, K. KEGG: new perspectives on genomes, pathways, diseases and drugs. *Nucleic Acids Res.* **45**, D353–D361 (2017).
63. Shen, X.-X. et al. Tempo and mode of genome evolution in the budding yeast subphylum. *Cell* **175**, 1533–1545 (2018).
64. Yang, Z. PAML 4: phylogenetic analysis by maximum likelihood. *Mol. Biol. Evol.* **24**, 1586–1591 (2007).
65. Popovic, M. Thermodynamic properties of microorganisms: determination and analysis of enthalpy, entropy, and Gibbs free energy of biomass, cells and colonies of 32 microorganism species. *Heliyon* **5**, e01950 (2019).
66. Heirendt, L. et al. Creation and analysis of biochemical constraint-based models using the COBRA Toolbox v.3.0. *Nat. Protoc.* **14**, 639–702 (2019).
67. Wang, H. et al. RAVEN 2.0: a versatile toolbox for metabolic network reconstruction and a case study on *Streptomyces coelicolor*. *PLoS Comput. Biol.* **14**, e1006541 (2018).
68. Yu, R. et al. Nitrogen limitation reveals large reserves in metabolic and translational capacities of yeast. *Nat. Commun.* **11**, 1881 (2020).

Acknowledgements

We acknowledge S. Viknander for giving feedback to improve this manuscript. This project received funding from the Novo Nordisk Foundation (grant no. NNF10CC1016517, J.N.), the Knut and Alice Wallenberg Foundation (J.N.) and the European Union's Horizon 2020 research and innovation programme with projects DD-DeCaF (grant no. 686070, J.N., F.L., H.L. and Y.C.) and SynBio4Flav (grant no. 814650, E.J.K.). The computations were enabled by resources provided by the Swedish National Infrastructure for Computing at Chalmers Centre for Computational Science and Engineering and High Performance Computing Center North, partially funded by the Swedish Research Council through grant agreement no. 2018-05973 (F.L. and Y.C.).

Author contributions

F.L., L.Y., H.L. and J.N. designed the research. F.L. and L.Y. performed the research. F.L., L.Y., Y.C., G.L., E.J.K. and J.N. analysed the data. L.Y. and M.K.M.E. collected the k_{cat} data. F.L., L.Y., H.L, G.L., Y.C., M.K.M.E., E.J.K. and J.N. wrote the paper. All authors approved the final paper.

Funding

Open access funding provided by Chalmers University of Technology.

Competing interests

The authors declare no competing interests.

Additional information

Supplementary information The online version contains supplementary material available at https://doi.org/10.1038/s41929-022-00798-z.

Correspondence and requests for materials should be addressed to Eduard J. Kerkhoven.

Peer review information *Nature Catalysis* thanks Dong-Yup Lee and the other, anonymous, reviewer(s) for their contribution to the peer review of this work.

nature research

Corresponding author(s): Eduard J Kerkhoven

Last updated by author(s): Apr 5, 2022

Reporting Summary

Nature Research wishes to improve the reproducibility of the work that we publish. This form provides structure for consistency and transparency in reporting. For further information on Nature Research policies, see our Editorial Policies and the Editorial Policy Checklist.

Statistics

For all statistical analyses, confirm that the following items are present in the figure legend, table legend, main text, or Methods section.

n/a	Confirmed	
□	☒	The exact sample size (*n*) for each experimental group/condition, given as a discrete number and unit of measurement
□	☒	A statement on whether measurements were taken from distinct samples or whether the same sample was measured repeatedly
□	☒	The statistical test(s) used AND whether they are one- or two-sided *Only common tests should be described solely by name; describe more complex techniques in the Methods section.*
☒	□	A description of all covariates tested
□	☒	A description of any assumptions or corrections, such as tests of normality and adjustment for multiple comparisons
□	☒	A full description of the statistical parameters including central tendency (e.g. means) or other basic estimates (e.g. regression coefficient) AND variation (e.g. standard deviation) or associated estimates of uncertainty (e.g. confidence intervals)
□	☒	For null hypothesis testing, the test statistic (e.g. *F*, *t*, *r*) with confidence intervals, effect sizes, degrees of freedom and *P* value noted *Give P values as exact values whenever suitable.*
□	☒	For Bayesian analysis, information on the choice of priors and Markov chain Monte Carlo settings
□	☒	For hierarchical and complex designs, identification of the appropriate level for tests and full reporting of outcomes
□	☒	Estimates of effect sizes (e.g. Cohen's *d*, Pearson's *r*), indicating how they were calculated

Our web collection on statistics for biologists contains articles on many of the points above.

Software and code

Policy information about availability of computer code

Data collection	The dataset used for deep learning model construction was extracted from the BRENDA and SABIO-RK database on 10 July 2020 by customized scripts via Application Programming Interface (API). The whole dataset is available in GitHub repository: https://github.com/SysBioChalmers/DLKcat/tree/master/DeeplearningApproach/Data/database. Literature collected experimental data used in the development of ecGEMs were stored in the supplementary file and the references were stated in the same file.
Data analysis	All code for the analysis and reproducing all figures are included in the GitHub repository: https://github.com/SysBioChalmers/DLKcat. The deep learning model processes uses Python based code, the version for the python packages: Python v3.7.6 (Anaconda installation recommended) PyTorch v1.4.0 scikit-learn v0.23.2 Biopython v1.78 RDKit 2020.09.1 seaborn v0.11.0 Matplotlib v3.3.2 pandas v1.1.3 SciPy v1.5.2 NumPy v1.20.2 dN/dS analysis used the Python based code, the version for the python package: PAML v4.7 The Bayesian learning approach uses Matlab code, the version for all Matlab packages are listed as below: MATLAB (R2019b) The COBRA toolbox for MATLAB (version 3.2).

The RAVEN toolbox (version 2.4.0)
The libSBML MATLAB API (version 5.17.0 is recommended).
Violinplot-Matlab (releases v0.1)
PVAL_ADJUST (2019.08.27)
IBM CPLEX(version 12.10)
Detailed instruction about the usage of those toolboxes were documented in the GitHub repository README file.

For manuscripts utilizing custom algorithms or software that are central to the research but not yet described in published literature, software must be made available to editors and reviewers. We strongly encourage code deposition in a community repository (e.g. GitHub). See the Nature Research guidelines for submitting code & software for further information.

Data

Policy information about availability of data

All manuscripts must include a data availability statement. This statement should provide the following information, where applicable:

- Accession codes, unique identifiers, or web links for publicly available datasets
- A list of figures that have associated raw data
- A description of any restrictions on data availability

Protein sequence FASTA files, deep learning predicted kcat values, GEMs, original-ecGEMs, DL-ecGEMs and Posterior-mean-ecGEMs for 343 yeast/fungi species are available as Supplementary Dataset on the Zenodo: https://doi.org/10.5281/zenodo.5797013. Collected proteome data are available in the GitHub repository (https://github.com/SysBioChalmers/DLKcat/tree/master/BayesianApporach/Data/Proteome_ref.xlsx). All other collected dataset such as the training dataset and the deep learning model were available in the GitHub repository: https://github.com/SysBioChalmers/DLKcat. Databases including BRENDA (https://www.brenda-enzymes.org), SABIO-RK (http://sabiork.h-its.org/) UniProt database (https://www.uniprot.org/), PubChem (https://pubchem.ncbi.nlm.nih.gov) were used in the DLKcat model reconstruction. KEGG (http://www.kegg.jp/) was used in the evaluation of the DLKcat performance. Databases including MetaNetX database (https://www.metanetx.org/), PDBe database (https://www.ebi.ac.uk/pdbe/) as well as the Complex Portal (https://www.ebi.ac.uk/complexportal) were used in the ecGEM reconstruction. The authors declare that all data supporting the findings and for reproducing all figures of this study are available within the paper and Supplementary files.

Field-specific reporting

Please select the one below that is the best fit for your research. If you are not sure, read the appropriate sections before making your selection.

☒ Life sciences ☐ Behavioural & social sciences ☐ Ecological, evolutionary & environmental sciences

For a reference copy of the document with all sections, see nature.com/documents/nr-reporting-summary-flat.pdf

Life sciences study design

All studies must disclose on these points even when the disclosure is negative.

Sample size

For the deep learning part, the dataset was randomly split into training, validation and test dataset by 80%, 10%, and 10%, respectively. The performance of the deep learning model was evaluated directly from the validation dataset, the testing dataset and the subset of the testing dataset without any assumption of underlying distributions. The sample size in the SMC-ABC part was chosen based on the computational power we have. We chose 126 samples per iteration for parallel purpose.

Data exclusions

In the section of data collection and preprocessing for deep learning model construction, we excluded the incomplete dataset that cannot be used in the deep learning model development. This part is described in the Methods.

Replication

For the deep learning approach, the model training process was repeated twice using the best hyperparameters after hyperparameter tuning to make sure our conclusions could be successfully reproduced. The SMC-ABC part was repeated once without specifying the random seed. All attempts at replication were successful. The conclusions in the manuscript was successfully reproduced. All scripts for reproducibility are included in the GitHub repository.

Randomization

As for the SMC-ABC approach, all values were randomly sampled from the Prior distribution without any seed.

Blinding

Not relevant with this computational study, but instead publicly available enzyme kinetics data from the BRENDA and SABIO-RK database was used.

Reporting for specific materials, systems and methods

We require information from authors about some types of materials, experimental systems and methods used in many studies. Here, indicate whether each material, system or method listed is relevant to your study. If you are not sure if a list item applies to your research, read the appropriate section before selecting a response.

Materials & experimental systems

n/a	Involved in the study
☒	□ Antibodies
☒	□ Eukaryotic cell lines
☒	□ Palaeontology and archaeology
☒	□ Animals and other organisms
☒	□ Human research participants
☒	□ Clinical data
☒	□ Dual use research of concern

Methods

n/a	Involved in the study
☒	□ ChIP-seq
☒	□ Flow cytometry
☒	□ MRI-based neuroimaging